Available online at www.sciencedirect.com
SCIENCE DIRECT®
International Journal of Thermal Sciences 44 (2005) 357–366
International Journal of Thermal Sciences
www.elsevier.com/locate/ijts

3-D time-dependent modelling of the plasma spray process. Part 1: flow modelling

Gilles Mariaux *, Armelle Vardelle

SPCTS-ENSIL, University of Limoges, 16, rue Atlantis, 87068 Limoges cedex, France

Received 20 February 2003; received in revised form 24 April 2004; accepted 9 September 2004

Available online 23 November 2004

Abstract

The plasma spray process is widely used to produce thick coatings by the successive pilling of particles deposited in a molten or semi-molten state on a prepared substrate. However, this process includes time-dependent phenomena that affect the reliability of the process and reproducibility of coating. These phenomena are principally linked to the continuous movement of the electric arc root on the anode wall in the plasma gun. Such a movement leads to arc length variations resulting in fluctuations in arc voltage, enthalpy input to the flow and instabilities in the plasma jet. This paper presents an attempt to develop a time-dependent and 3-D model of the plasma spray process that can provide a useful insight in the time-evolution of the performance of the process. The effect of the transient behaviour of the arc on the gas flow is modelled with a time dependant heat source located inside the nozzle and evolving with the arc voltage. The first stage of the study consisted in the validation of the flow model thanks to the comparison of steady-state computed results with experimental data. The second dealt the time-dependant simulation of the flow.

Keywords: Plasma spraying; Flow; Unsteady; 3-D; Arc; Modelling

1. Introduction

Plasma spraying is used to deposit thick coatings of metals, ceramics, polymers and composites for engineering applications [1,2]. The latter include automotive and gas-turbine components, pulp and paper processing, steel industry, corrosion and erosion protection, biomedical implants and so on.

This process uses a non-transferred dc plasma torch in which the plasma-forming gas is fed between the concentric water-cooled copper anode and tungsten cathode as shown in Fig. 1. The gas is heated by Joule effect when passing through the electric arc that strikes between electrodes. At the nozzle exit, the gas temperature is generally higher than 12 000 K and the velocity can reach 2 000 $m \cdot s^{-1}$ because of the gas expansion. The torch power level generally ranges between 10 and 80 kW. However, about 30 to 40% of the electric power input to the gas is lost in the cooling system of the electrodes. In addition, the arc root moves on the anode surface under the combined action of the drag force exerted by the flow and the Lorentz forces and this movement induces variations in the arc length and, therefore, in arc voltage. Such variations result in fluctuations in the enthalpy input to the gas and affect the flow fields as well as the heating and acceleration of the particles injected in the plasma jet. As the development of dedicated and time-resolved experiments can be difficult, a time-dependent model able to predict the effect of the torch operating conditions on the flow fields, in-flight particle behaviour and coating formation would be a useful tool to have a better understanding of the transient phenomena occurring during the spray process.

The modelling of this deposition process has received considerable attention during the last years and various models have been proposed in the literature [3–8]. However, if

* Corresponding author. Tel.: +33 5 55 42 36 70, fax: +33 5 55 42 36 80.
E-mail address: mariaux@ensil.unilim.fr (G. Mariaux).

1290-0729/$ – see front matter
doi:10.1016/j.ijthermalsci.2004.07.006

Nomenclature

C_p	specific heat at constant pressure	$J \cdot kg^{-1} \cdot K^{-1}$	
D_i	diffusivity of species i	$m^2 \cdot s^{-1}$	
$f_{x,y,z}$	force vector component per unit mass	$m \cdot s^{-2}$	
G_k	production term of turbulent kinetic energy	$kg \cdot m^{-1} \cdot s^{-3}$	
H	specific enthalpy	$J \cdot kg^{-1}$	
I	arc current	A	
I_t	turbulence intensity	%	
k	turbulent energy per unit mass of fluid	$m^2 \cdot s^{-2}$	
L_m	turbulent mixing length	m	
m	mass fraction		
n	coordinate normal to the domain boundary	m	
p	static pressure	Pa	
P	arc power	W	
Pr_t	turbulent Prandtl number		
q_m	mass flow rate	$kg \cdot s^{-1}$	
r	radius	m	
R_{torch}	plasma torch nozzle radius	m	
Sc_t	turbulent Schmidt number		
S_φ	source term of variable φ		
T	temperature	K	
v	velocity	$m \cdot s^{-1}$	
V	arc voltage	V	

Greek symbols

φ	variable	
Γ_φ	transport coefficient	
ε	rate of dissipation of turbulent energy	$m^2 \cdot s^{-3}$
μ	dynamic viscosity	$kg \cdot m^{-1} \cdot s^{-1}$
μ_t	turbulent dynamic viscosity	$kg \cdot m^{-1} \cdot s^{-1}$
ν	kinematic viscosity	$m^2 \cdot s^{-1}$
κ	thermal conductivity	$W \cdot m^{-1} \cdot K^{-1}$
η	plasma torch thermal efficiency	%
ρ	density	$kg \cdot m^{-3}$
τ	coordinate tangent to the domain boundary	m

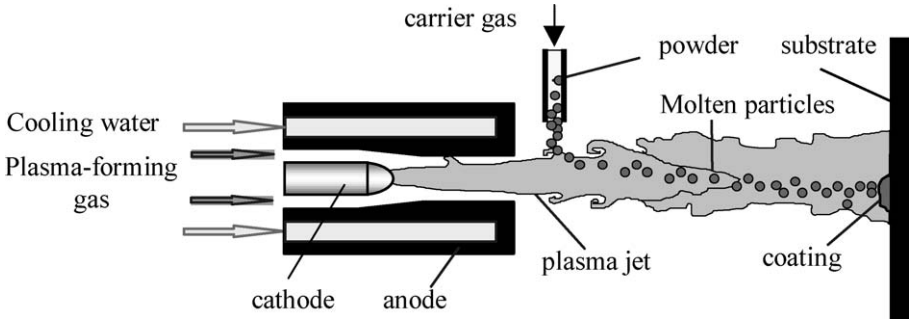

Fig. 1. Schematic illustration of the plasma spray process.

they adopt practically the same methodology for the calculation of the turbulent plasma jet and particle behaviour, very little deal with transient phenomena as plasma formation in the nozzle [9–11] and flow fluctuations.

This paper presents a tri-dimensional and time-dependent model of the jet formation and mixing with the surrounding atmosphere. A very simple model of the plasma jet formation based on a transient volume heat source located within the nozzle is used to model the conversion from electrical to thermal energy in the plasma-forming gas.

After a brief description of the operation of a dc plasma torch and sets of spraying conditions used in calculations, the first part will present the main characteristics of the model. The second part will discuss the validation of the computed results from experimental data prepared under the same spraying conditions. However, as these data are time averaged, the comparison deals with steady state predictions. Finally, the third part will present the predictions got with the unsteady state models.

2. Operation of a dc plasma torch

2.1. Arc operation mode

The operation of a dc plasma torch is characterized by the movement of the arc root on the anode wall and, therefore, in the time-evolution of the arc voltage. Wutzke and al. have identified three main arc operation modes [12]: the steady mode, the takeover mode and the restrike mode. In the first mode, no distinct motion of the arc root is observed while in the take over mode, the motion of the arc is more random and occasionally, two simultaneous anode attachment spots can be observed. Finally, the restrike mode is characterized by strong fluctuations of arc movement and very steep voltage drops. Duan and Heberlein [13] have shown that the operation mode depends on the thickness of the cold gas boundary layer that develops at the anode wall and various authors have found that the boundary layer thickness depends essentially on the torch geometry, plasma-forming

gas nature and flow rate, gas injection mode and arc current intensity [13–15].

Gas mixtures of argon and hydrogen (10–25% vol) are generally used to spray refractory materials as ceramics: in a schematic way, the argon gas helps to stabilize the arc column and ensures the acceleration of the particles while the hydrogen gas that has a high thermal conductivity and specific enthalpy, ensures the heating and melting of particles. Such mixtures give rise to arcs operating in the restrike mode with a rather thick cold gas boundary layer at the anode wall ($\sim$ 1–2 mm). The voltage time-evolution exhibits a saw-tooth shape with a rather well identified fundamental period as shown in Fig. 2. Indeed, the arc is stretched by the cold gas flow until an electric breakdown occurs through the colder and electrically insulating layer surrounding the arc. Each breakdown initiates a short circuit and a new arc attachment at the nozzle wall [13]. The frequency of arc fluctuations usually ranges between 2 and 20 kHz and the voltage amplitude can fluctuate by more than 20% about the average value. The frequency and amplitude of the arc fluctuations evolve with the wear of the anode that causes an increase in the roughness of the wall and favours the striking of the arc at specific locations.

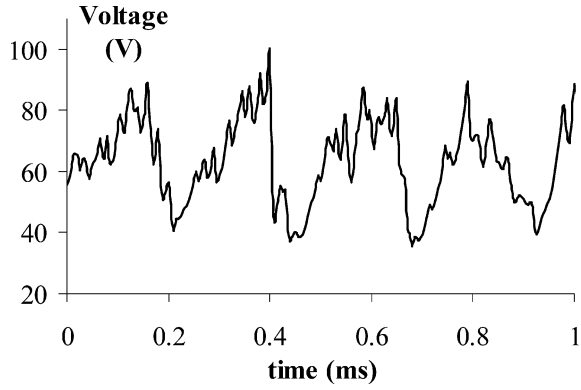

Fig. 2. Time-evolution of the torch voltage (from Bisson et al. [19]). F4-MB plasma torch. Gas mixture: 35 slm of Ar and 10 slm of H_2. Arc current: 550 A (see spray condition set "SP_{SM}" of Table 1).

2.2. Plasma spraying conditions used in the study

The calculations were performed with the two different sets of spraying parameters listed in Table 1. Both combined a high arc current and hydrogen content in order to favour the restrike mode for the arc movement.

For the first set of operating parameters, named as "SP.lab" a comprehensive database of experimental data of plasma jet temperature, velocity and composition is available at the Laboratory [16–18]. However, as the measurement techniques (emission spectroscopy, enthalpy probe, ...) provided time-averaged data, steady-state calculations of the spray process were also performed to validate the results of the computational model.

The second set of spraying parameters, named as "SP_{SM}", was utilized to study the effect of the arc voltage fluctuations on the plasma flow field. These conditions were similar to the conditions used by Bisson et al. [19] to experimentally observe the transient behaviour of particles in a fluctuating plasma jet.

3. Modelling of the plasma jet issuing in air

3.1. Model assumptions

A realistic model of the plasma spray process should be three-dimensional to enable the taking into consideration of the motion of the arc inside the plasma torch, transverse injection of the powder, effect of the carrier gas on the plasma jet and three-dimensional character of turbulence [20]. Even if this study is restricted to the plasma flow and uses an external injector for the powder that is supposed to perturb very little the plasma flow compared to an internal injection, a tri-dimensional geometry was used. Indeed, this model is

Table 1
Plasma spaying parameters

Plasma torch parameters		
Plasma gun	"SP_{SM}": F4-MB	"SP.lab": Lab'torch
Plasma-forming gas	35 slm Ar + 10 slm H_2	45 slm Ar + 15 slm H_2
Torch nozzle exit	7 mm	7 mm
Gas mass flow rate	9.28×10^{-4} kg·s^{-1}	1.25×10^{-3} kg·s^{-1}
Arc current	550 A	600 A
Mean voltage	62.5 $V_{(min: 30V\, max: 105\, V)}$	65 V
Mean effective power	19250 W	21450 W
Mean thermal efficiency	56%	55%
Environment	Air at atmospheric pressure	
Powder injection		
Location of injector	Vertical, 6 mm downstream of the nozzle exit and 9 mm away from the jet centerline	Vertical, 4 mm downstream of the nozzle exit and 8.5 mm off torch centerline
Injector diameter	1.5 mm	1.8 mm
Carrier gas	Ar, 3 slm	Ar, 6 slm

a part of a "global" model under development at the Laboratory. This model involves the modelling of the arc formation and motion inside the nozzle by coupling the flow equations and the electromagnetism equations [21,22], internal injection of the ceramics powder and coating formation on the substrate [11,23].

The modelling of the plasma jet issuing in air was based on the following assumptions:

- The local thermodynamic equilibrium (LTE) prevailed in the internal and external flows, that is to say the molecules, atoms, ions and electrons have the same temperature [24]. This assumption is generally accepted in the modelling of atmospheric plasma jets. However, it is questionable in the zones with steep temperature gradients (zones close to the electrodes ...) and it should be removed in further development.
- the medium was [25] considered as a continuum;
- the fluid was Newtonian and the plasma optically thin [24];
- no demixion and chemical reactions occurred in the gas phase. This assumption is contestable for a plasma flow of argon and hydrogen issuing in air, as the oxygen of air can react with nitrogen and hydrogen. However, the heat produced by the oxidation reactions in the gas phase is low compared to that input by the electric arc. Moreover, the present model is used for the prediction of the plasma spraying of ceramics for which the chemical reactions with the gas phase are generally limited compared to that undergone by metal particles that can be subjected to chemical reactions with oxygen or other oxidizing species such as OH [26].
- the flow was subsonic. Preliminary calculations have shown that, under the spraying conditions of the study, the Mach number was maximum inside the plasma torch and was less than 0.6.
- the gas was supposed to be made up of three components: the plasma-forming gas, the powder carrier gas and the ambient gas.

3.2. Mathematical equations

The model used the conservation equations of mass, species, momentum, energy and turbulence written in 3-D Cartesian coordinates. Equations were solved by using the commercial CFD code Estet 3.4. The latter [27] is a software package dedicated to steady or unsteady, subsonic, turbulent, multi-component reactive or multi-phase flows. It uses a numerical hybrid scheme combining finite difference and finite volume methods applied to a mono-bloc structured mesh grid [27] (SIMPLEC Algorithm [28]).

The conservation equations for the mean turbulent flow were expressed as follow:

$$\frac{\partial(\rho\varphi)}{\partial t} + \operatorname{div}(\rho\varphi\mathbf{v}) = \operatorname{div}(\Gamma_\varphi \,\mathbf{grad}\,\varphi) + S_\varphi$$

where φ, Γ_φ and S_φ are a specific variable, the corresponding transport coefficient and source term, respectively. They are summarized in Table 2 for the various equations.

Due to the large temperature range (300 to 13 000 K) in the calculation domain, the properties of the different gas are subjected to large variations enhanced by gas dissociation and ionisation [24]. The thermodynamic (density, specific heat and specific enthalpy) and transport properties (viscosity and thermal conductivity) of the gas mixture were calculated in terms of local composition and temperature using the mixing laws and the temperature-dependent properties of each gaseous component (carrier gas, plasma gas, ambient air). These laws were expressed in terms of the mass fraction or molar fraction of each gas [25,29,30] and did not take into account possible chemical reactions between the various gases, according to the assumptions of the model (Section 3.1). Therefore, the physical properties of each gas take into account ionization and chemical reactions.

Table 2
Transports coefficients and source terms for the equation of the averaged flow (average operator is implicit)

φ	Γ_φ	S_φ
1	0	$\operatorname{div}(\rho\mathbf{v})$
u	$\mu_{eff} = \mu + \mu_t$	$-\frac{\partial p}{\partial x} + \rho f_x + \operatorname{div}(\mu_{eff}\frac{\partial \mathbf{v}}{\partial x}) + \frac{\partial}{\partial x}(-\frac{2}{3}\mu_{eff}\operatorname{div}\mathbf{v}) - \frac{2}{3}\frac{\partial}{\partial x}(\rho k)$
v	μ_{eff}	$-\frac{\partial p}{\partial y} + \rho f_y + \operatorname{div}(\mu_{eff}\frac{\partial \mathbf{v}}{\partial y}) + \frac{\partial}{\partial y}(-\frac{2}{3}\mu_{eff}\operatorname{div}\mathbf{v}) - \frac{2}{3}\frac{\partial}{\partial y}(\rho k)$
w	μ_{eff}	$-\frac{\partial p}{\partial z} + \rho f_z + \operatorname{div}(\mu_{eff}\frac{\partial \mathbf{v}}{\partial z}) + \frac{\partial}{\partial z}(-\frac{2}{3}\mu_{eff}\operatorname{div}\mathbf{v}) - \frac{2}{3}\frac{\partial}{\partial z}(\rho k)$
H	$\rho(\kappa/C_p.\rho) + \mu_t/Pr_t$	$S_H + \boldsymbol{v}.\mathbf{grad}\,p$
m_i	$\rho.D_i + \mu_t/Sc_t$	0
k	$\mu + \mu_t/\sigma_k$	$-\frac{2}{3}\rho k\operatorname{div}\mathbf{v} - \frac{2}{3}\mu_t(\operatorname{div}\mathbf{v})^2 + G + \rho(G_k - \varepsilon)$
ε	$\mu + \mu_t/\sigma_\varepsilon$	$-\frac{2}{3}C_{\varepsilon_1}\rho\varepsilon\operatorname{div}\mathbf{v} - \frac{2}{3}\mu_t C_{\varepsilon_1}\frac{\varepsilon}{k}(\operatorname{div}\mathbf{v})^2 + \rho\frac{\varepsilon}{k}(C_{\varepsilon_1}G_k - C_{\varepsilon_2}\varepsilon) + \frac{\varepsilon}{k}C_{\varepsilon_1}C_{\varepsilon_3}G$

$G_k = \frac{\mu_t}{\rho}[2(\frac{\partial u}{\partial x})^2 + 2(\frac{\partial v}{\partial y})^2 + 2(\frac{\partial w}{\partial z})^2 + (\frac{\partial u}{\partial y} + \frac{\partial v}{\partial x})^2 + (\frac{\partial u}{\partial z} + \frac{\partial w}{\partial x})^2 + (\frac{\partial v}{\partial z} + \frac{\partial w}{\partial y})^2]$

$G = -\frac{1}{\rho}\frac{\mu_t}{\sigma_k}\frac{\partial \rho}{\partial x_i}\rho f_i; \qquad \mu_t = \rho C_\mu \frac{k^2}{\varepsilon}$

for the standard k–ε model:
$C_\mu = 0.09$; $C_{\varepsilon 1} = 1.44$; $C_{\varepsilon 2} = 1$; $C_{\varepsilon 3} = 1$ if G > 0, else 0; $\sigma_k = 1.92$; $\sigma_\varepsilon = 1.30$

In addition, temperature-enthalpy tabulations were used to infer the temperature from the predicted enthalpy of the multi-component gas mixture.

3.3. Turbulence model

The rates of diffusion of heat, momentum and species in the plasma flow are determined, to a great extent, by the level of turbulence and the way this turbulence is modelled. The arc fluctuations enhance the development of the turbulence that starts at the jet border where it comes into contact with the ambient gas at rest.

In this study, two k–ε turbulence models were used. The first model included the correction of Launder and Sharma [31] at low Reynolds numbers. In the second model, the k and ε equations were derived from the application of a rigorous statistical technique (issued from the ReNormalization Group (RNG) theory) to the Navier–Stokes equations [32]. It is comparable to the standard k–ε model in its form but includes an additional term in the dissipation equation. This term increases significantly the dissipation for flows with large shear stress rate like deviated or separated flow.

If the k–ε model is not really satisfactory for non-isotropic, non-fully turbulent flows with a large range of turbulence scales, it was, however, used in this study to obtain reasonable CPU times.

Moreover, a previous study [33] dealing with a turbulent model based on the transport of Reynolds Stresses (RSM, $R_{ij} - \varepsilon$) showed no significant differences between this model and the k–ε model, even when the mesh grid was refined, the domain size increased and the simulation performed in unsteady state.

3.4. Calculation domain

Fig. 3 shows the computational domain ($42 \times 125 \times 42$ mm^3), boundary conditions and Cartesian grid used in this study. The size of the calculation domain and mesh grid resulted from preliminary calculations dedicated to the study of the effect of domain geometry on plasma flow fields [25]. The numerical grid consisted of 147 825 nodes: 45, 73 and 45 in the x-, y- and z-direction, respectively, with a finer mesh close to the anode wall. The computational domain included the torch nozzle in the internal field and the plasma free jet and injection of the powder carrier gas in the external field.

3.5. Models of the arc fluctuations

Two different models were used to model the gas heating inside the nozzle and the effect of the arc fluctuations on the plasma jet behaviour.

The first model [34] (named as "V&T") consisted in imposing the velocity and temperature profiles at the nozzle exit (index 3 in Fig. 3). The later were drawn from experiments. When using the "SP.lab" operating conditions [25], the measured steady-state gas velocity and temperature profiles $v(r)$ and $T(r)$ at the torch exit could be expressed respectively as: $v(r) = v_{\max}(1 - (r/R_{\text{torch}})^2)$ and $T(r) = (T_{\max} - T_{\text{anode}})(1 - (r/R_{\text{torch}})^{4.5}) + T_{\text{anode}}$ [35], where $v_{\max}$ and $T_{\max}$ are the maximum velocity and temperature on the torch axis and T_{anode} was fixed at 1000 °C (temperature close to the melting point of copper).

This model was used for steady state simulations in this study but it had already been extended to an unsteady flow in a previous work [33]. The main weakness of this model is to require experimental data established under the same operating conditions than the conditions used in calculations. Moreover, the experimental data are generally time-averaged and an additional assumption is necessary to generate time-dependent boundary conditions from these data.

The second model (labeled "PV", for Volume Power) used a time-dependent volumetric heat source (W·m^{-3}) imposed in a fixed portion of the nozzle (Fig. 3, index 2) to model the conversion from electrical to thermal energy in the plasma-forming gas. This volume power was drawn from the instantaneous electric power, $V(t) \times I$, divided by the volume of the cylindrical portion of the nozzle in which the electric power was released (Fig. 3, index 2). The diameter of the cylinder was equal to the diameter of the nozzle and its length was adjusted so that the predicted thermal torch ef-

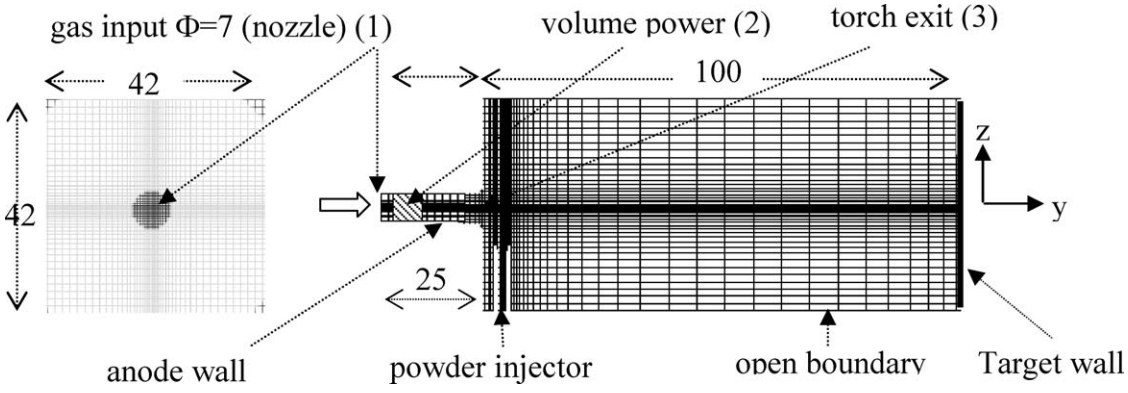

Fig. 3. Calculation domain, grid and boundaries (all dimensions are in millimeters).

Table 3
Boundary conditions

	Inlet	Wall	Open boundary
Velocity v	$v(r) = v_{\max}.(1-(r/R_{\text{torch}})^2)$	$v = 0$	$\frac{\partial v_{\tau \text{ and } n}}{\partial n} = 0$
Enthalpy H	"V&T model" $H = H(r)$	Anode	If $v_n > 0$
		"V&T model"	(outgoing v):
	"PV model" H_{ArH_2}(300 K)	$\frac{\partial H}{\partial n} = 0$	$\frac{\partial H}{\partial n} = 0$
		"PV model" $H = H_{\text{ArH2}}$ (1273 K)	else
			$H = H_{\text{air}}$ (300 K)
Pressure	Calculated	$\frac{\partial p}{\partial n} = 0$	If $v_n > 0$: $p = p_\infty$ else
			$p + \rho V^2/2 = p_\infty$
			or $\frac{\partial}{\partial n}(\frac{\partial p}{\partial \tau}) = 0$
Mass fraction m	$m_{\text{ArH2}} = 1$	$\frac{\partial m_i}{\partial n} = 0$	$v_n > 0$: $\frac{\partial m_i}{\partial n} = 0$
			else $m_{\text{Air}} = 1$
Turbulence k, ε	$k(r) = 0.5(I_t v(r))^2$		If $v_n > 0$ $\frac{\partial k_{or}\varepsilon}{\partial n} = 0$
	"V&T model" [6]:	$k = 0$	else
	$\varepsilon(r) = C_\mu \frac{k(r)^{1.5}}{L_m}$	$\frac{\partial \varepsilon}{\partial n} = 0$	$k = \varepsilon = 0$
	$L_m = 0.075 R_{\text{torch}}$; $C_\mu = 0.09$		
	"PV model" [38]:		
	$\varepsilon(r) = C_\mu k(r)^2/(10v)$		

ficiency was equivalent to the one measured under the same spraying conditions. For the two sets of spraying parameters used in calculations (Table 1), it was found that a cylinder length of 6.1 mm leads resulted in a good estimate of the thermal efficiency of the torch.

The same volumetric power value was imposed in each cell of the cylinder and was taken into account as a source term in the equation of energy. At the entrance of the nozzle (Fig. 3, index 1), the plasma-forming gas temperature was set at 27 °C and the gas velocity profile was laminar with an angle taking the conic shape of the cathode. The heat transfer to the anode was modelled using the classical "law of the wall" [36] and assuming that the surface temperature of the anode was maintained at a constant temperature of 1000 °C.

This model of the conversion from electrical to thermal energy in the plasma gas did not allow the prediction of the dynamic behaviour of the arc that requires the solution of the [37] Magneto-Hydro-Dynamic equations [21,22]. However, it made it possible to have realistic projections of the flow fields by using as sole input data the arc current, arc voltage time-evolution and torch thermal efficiency.

It should be noted that such a model based on an energy source term in the heat equation to predict the heating of the gas in the torch, has been used in steady-state conditions by various authors as Eichert [38] and Remesh et al. [39]. The former have carried out a detailed study of the effect of some parameters of the model (volumetric power intensity, heat transfer to the anode wall, ...) with the PHOENICS CFD code. The latter used this model to study the behaviour of particles injected in the gas flow with FLUENTv5.01 code.

3.6. Boundary conditions

Turbulence conditions at domain inlet. The turbulence boundary conditions consisted in the inflow radial profiles of the turbulent kinetic energy, $k(r)$ and its dissipation rate, $\varepsilon(r)$ (r is the distance to the torch axis). The former was calculated from the gas velocity profile at the domain inlet $v(r)$ (index 1 or 3, Fig. 3) and the turbulence intensity, I_t, set at 2% [38]: $k(r) = 0.5(I_t v(r))^2$.

The dissipation rate profile $\varepsilon(r)$ was deduced from the profile of $k(r)$ and is given in Table 3.

Shear stress and heat transfer to the anode wall. Close to the anode wall, the mesh grid of the calculation domain was refined in such a way that the nearest node to the wall was located in the viscous sub-layer. The mesh grid is composed of 19×19 nodes in the $x - z$ plan inside the torch.

The shear stress at the wall surfaces was predicted by modelling, with the classical "log-law of the wall", the velocity in the boundary layer that develops at the wall surface [36]. The temperature distribution in this boundary layer was deduced from the velocity distribution using the analogy of Prandtl–Taylor [40].

The whole boundary conditions are resumed in Table 3.

4. Results and discussion

Two successive sets of numerical calculations have been conducted.

- The first set dealt with the steady-state calculations of the plasma flow under the so-called "SP.lab" operating conditions of the plasma torch. It used either imposed gas velocity and temperature profiles at the nozzle exit or a heat source in the nozzle to model the plasma formation. The predictions were compared with time-average experimental data obtained under the same spraying conditions.
- The second was dedicated to the unsteady-state calculations of the plasma flow under the "SP_{SM}" plasma operating conditions.

4.1. Steady-state flow calculations

Fig. 4 shows a comparison of the predicted and experimental radial velocity profiles at 2 mm downstream of the nozzle exit under the spraying parameters "SP.lab". The predictions got with the model using imposed velocity and temperature profiles at the domain inlet ("V&T" model) are in good agreement with the experimental data whereas the profile obtained with the volume heat source model ("PV" model) is flatter than the experimental one. This difference may be explained by the assumption of a uniform volumetric heat source inside the nozzle. However, the agreement between the numerical and experimental radial profiles of the gas temperature at the nozzle exit is good for both "V&T" and "PV" models as, above 10 000 °C, most of the enthalpy input to the gas is used in the ionisation process and a large variation in gas enthalpy is required to give rise to a notable change in gas temperature.

It should be noticed that, even if the heat source model does not take into account the physics of arc formation, it provides, in a simple way, a rather good estimate of the gas velocity and temperature at the nozzle exit from the operating parameters of the spray torch. Nevertheless, the output results depend to a great extent on the size of the volume in which the conversion from electrical to thermal energy takes place as it conditions the heat power transferred to the anode wall and input in the plasma-forming gas. As explained in Section 3.4, the comparison between the predicted and measured thermal efficiency of the torch makes it possible to adjust the size of this volume. Another method to estimate the pertinent length of this volume would be to use a 1-D model of enthalpy conservation in the arc column [41].

Figs. 5 and 6 show the measured and calculated variation of the gas velocity and temperature along the jet centreline. The numerical simulations were carried out with the "PV model" and "V&T model" and two k–ε turbulence models. From these figures, it can be seen that:

- the velocity and temperature of the gas exhibit a drastic increase inside the nozzle as the conversion from electrical to thermal energy proceeds,
- the predictions obtained with the gas profiles imposed at the nozzle exit ("V&T" model) are similar to those obtained with the volume heat source model ("PV" model) provided that the same turbulence model is used, even if the initial conditions for turbulent dissipation (ε) are defined differently in both arc representation (Table 3). The minor differences in the velocity and temperature evolutions are probably due to a variation by 10% in the gas velocity at the nozzle exit.

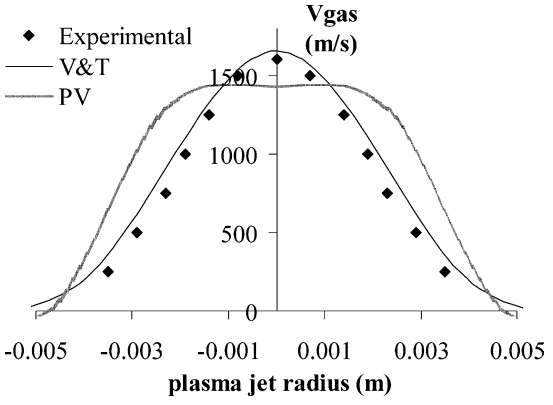

Fig. 4. Comparison between measurements and predictions of the gas velocity profile at 2 mm from the nozzle exit. Predictions were obtained with the "V&T" and "PV" models. Spraying conditions: "SP.lab" (Table 1).

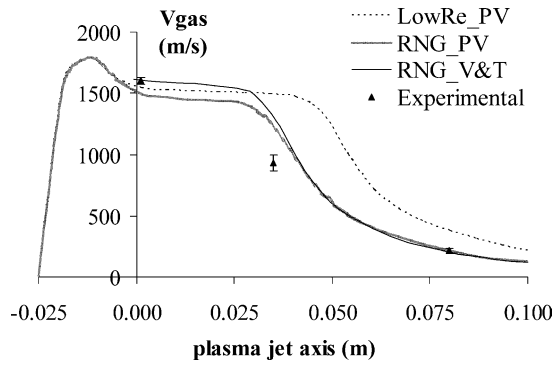

Fig. 5. Predicted and experimental centerline profiles of the gas velocity. Both the "V&T" and "PV" models were used for the computations with two k–ε turbulence models. Spraying conditions: "SP.lab" (Table 1).

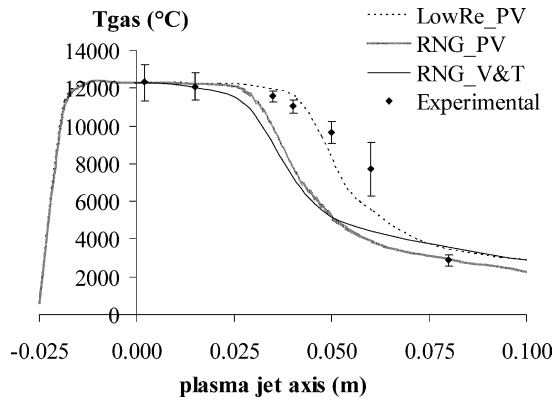

Fig. 6. Predicted and experimental centerline profile of the gas temperature. Both the "V&T" and "PV" models were used for the computations with two k–ε turbulence models. Spraying conditions: "SP.lab" (Table 1).

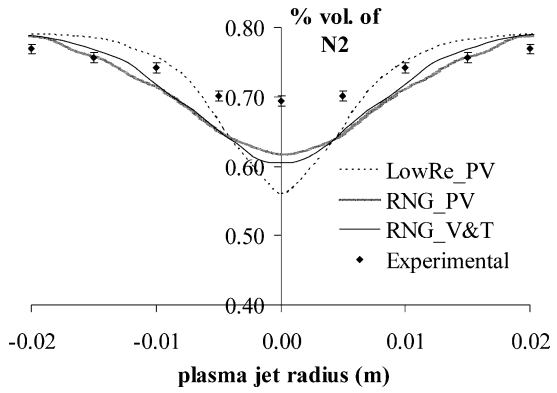

Fig. 7. Comparison between measurements and predictions of the nitrogen content in the gas flow at 80 mm from the nozzle exit. Both the "V&T" and "PV" models were used for computations with two k–ε turbulence models. Spraying conditions: "SP.lab" (Table 1).

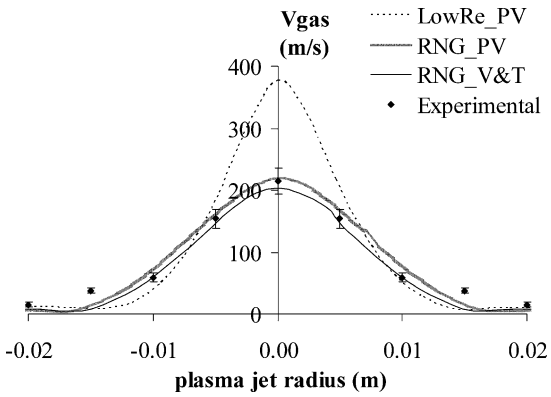

Fig. 8. Comparison between measurements and predictions of the gas velocity profile at 80 mm from the nozzle exit. Both the "V&T" and "PV" models were used for computations with two k–ε turbulence models. Spraying conditions: "SP.lab" (Table 1).

The main differences between the results of these three calculations arise from the transition to turbulence which occurs further downstream in the gas flow when using the low Reynolds k–ε model as shown by the variation of the turbulence intensity as a function of the distance from the nozzle exit. With this turbulence model, the potential core of the gas jet is longer as the mixing of the plasma gas with the ambient gas is less efficient. Therefore, the decrease in gas temperature occurs further downstream.

The comparison between the predictions got with the 2 turbulence models points out that the gas temperature projected with the low-Reynolds turbulence model is in fair agreement with the experimental data while the gas velocity calculated with the RNG turbulence model agrees better with the experimental velocity data. However, both models overestimate the cooling of the gas whereas the mixing with the ambient gas is underestimated as shown in Fig. 7. The latter displays the nitrogen content in the plasma flow at 80 mm from the nozzle exit. The mixing of the plasma gas with the quiet and colder atmosphere is most likely not well predicted by the k–ε turbulence models.

The experimental and predicted profiles of gas velocity at 80 mm downstream from the nozzle exit (Fig. 8) confirm the previous observations that is the gas velocity projected with k–ε RNG turbulence model is in good agreement with the experimental velocity whereas the velocity provided by the low-Reynolds turbulence model is overestimated by 150 $\mathrm{m{\cdot}s^{-1}}$. The radial predicted temperature profiles exhibit a better agreement with measurements when calculated by using the RNG turbulence model except when a heat source is taken into account inside the torch nozzle.

As shown by the comparison with the measurements of the nitrogen content at 80 mm from the nozzle exit (Fig. 7), the mixing of the plasma gas with the surrounding air is underestimated by 15% with the RNG turbulence model. This disagreement is more marked with the low-Reynolds turbulence model for which the transition to turbulence occurs further downstream in the plasma jet.

The comparison of the predicted results with the experimental data show that, generally speaking, the k–ε RNG turbulence model provides predictions that are rather well representative of the actual flow plasma fields except for the cooling of the jet. This turbulence model allows a better control of the turbulent viscosity whereas the low-Reynolds turbulence model is more suitable close to walls.

However, a Large Eddy Simulation model coupled to the modelling of arc fluctuations should be more appropriate to model the large structures that arise from the difference in velocity and density of the plasma gas and ambient gas, and are enhanced by the arc fluctuations. Nevertheless, the k-ε model makes it possible to have reasonable calculation times, even with unsteady-state simulations.

4.2. Unsteady flow calculations

The unsteady flow calculations were performed with the spraying parameters "$\mathrm{SP_{SM}}$" of Table 1, a volumetric heat source inside the nozzle and the k–ε RNG turbulence model.

For the "$\mathrm{SP_{SM}}$" spray conditions, the arc voltage $V(t)$ evolved according to a saw tooth-shaped curve (Fig. 2) [19], around a mean value of 62 V with an amplitude ($2.\Delta V$) of 72 V. The frequency of fluctuation was 4.2 kHz. Such variation can be easily modelled by a periodic function.

The time-evolution of the electric power ($I.V(t)$), efficient electric power, gas velocity and temperature on the jet centreline at the torch exit are shown in Fig. 9. All these parameters vary as $V(t)$. The variation of the electric power ($V(t).I$) input to the gas ranges between 17600 and 56800 W and the power available at the torch exit between 10360 and 33550 W. It corresponds to a quasi-constant torch thermal efficiency of 58%, very close to the experimental one (55%). The gas velocity on the torch centerline at the nozzle exit varies between 800 and 1760 $\mathrm{m{\cdot}s^{-1}}$ and, the temperature between 11 040 and 14 350 °C. The narrower range in temperature fluctuations is explained by the gas ionisation that absorbs most of the enthalpy input to the flow.

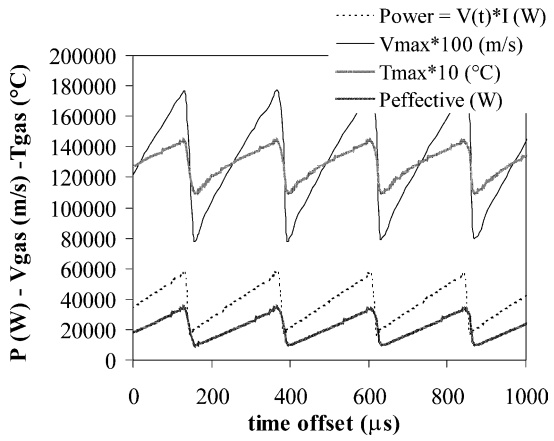

Fig. 9. Time-evolution of input and effective electric power, gas velocity and temperature at nozzle exit on jet centerline with the "PV" model. Spraying conditions: "SP_{SM}" (Table 1).

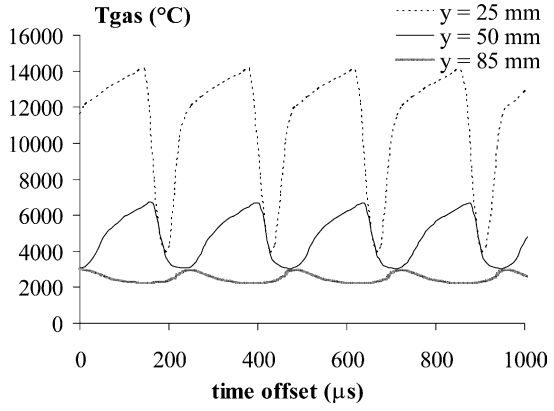

Fig. 10. Time-evolution of the gas centerline temperature at various distances from nozzle exit with the "PV" and k–ε RNG turbulence models. Spraying conditions "SP_{SM}" (Table 1).

Fig. 10 shows the time-evolution of the centreline gas temperature at 25, 50 and 85 mm from the nozzle exit. As expected, these curves exhibit a rapid decrease in fluctuation amplitude as the distance from the nozzle exit increases and the transition to turbulence proceeds. The amplitude of fluctuation (ΔT) is about 3300 °C at the nozzle exit; it increases up to 10 200 °C at 25 mm and decreases to 3600 °C at 50 mm and 730 °C at 85 mm. This corresponds to a relative fluctuation ($\Delta T(y)/T_{\text{mean\_}y=0}$) of 26%, 80%, 28% and 6%, respectively. These fluctuations are not noticeable any more at 85 mm from the nozzle exit.

The corresponding fluctuation in gas velocity (Δv) is equal to 970 $\text{m}\cdot\text{s}^{-1}$ at the nozzle exit; it increases up to 1120 $\text{m}\cdot\text{s}^{-1}$ at 25 mm, and decreases down to 610 $\text{m}\cdot\text{s}^{-1}$ at 50 mm and 95 $\text{m}\cdot\text{s}^{-1}$ at 85 mm. It corresponds respectively to a relative fluctuation ($\Delta v(y)/v_{\text{mean\_}y=0}$) of 76%, 88%, 48% and 7%, respectively.

The increase in the fluctuation amplitude occurs in the laminar zone of the jet whereas the decrease corresponds to the transition to turbulence. The diminution speeds up as the mixing of the plasma gas with the ambient gas proceeds. The shape of the curves is affected by the gas dissociation process that affects the relation between the gas enthalpy and temperature and, therefore, modify the density and velocity of the plasma jet.

The numerical simulations show that the amplitude of the fluctuations of the gas velocity and temperature is high and, thus, can significantly affect the acceleration and heating of the particles injected in the flow.

5. Conclusion

In this paper a 3D and time dependant model is presented to study the effect of the arc root fluctuations on the plasma flow. On the basis of this numerical study of the plasma flow, the following conclusions can be drawn:

- The simulation of the conversion from electrical to thermal energy inside the nozzle by a simple heat source in the energy equation, makes it possible to calculate the flow fields outside the torch by using the sole parameters fixed by the operator. However, this approach requires an accurate calculation of the heat transfer to the anode wall and the "right" length of the volume in which the heat conversion proceeds. The pertinent length can be adjusted from the comparison of the experimental and predicted thermal torch efficiency. However, the use of a 1-D energy balance in the arc column could be a better method to determine an approximate value of this length.
- The comparisons with experimental data show that the k-ε turbulence model predicts a too fast cooling of the plasma jet even though the mixing of the plasma gas with the surrounding gas is underestimated. Nevertheless, the agreement between calculated and measured gas velocity, temperature and air content is reasonable considering the assumptions of the model and the accuracy of measurements. A Large Eddy Simulation model coupled to the modelling of arc fluctuations should be more appropriate to model the large structures arising from the difference in velocity and density between the plasma gas and the ambient gas.
- Finally, the calculations show that the flow fields are subjected to important time-variations close to the nozzle exit. Therefore, it can be anticipated that parameters of the particles at impact will dependent on the instant they are injected in the plasma flow, as it will be experimentally and numerically shown in a next paper.

In the present state, the model presented in this paper can help to have a better understanding of the effect of operating parameters on plasma flow parameters. The implementation in this model of the electric arc behaviour is in progress. This requires the simultaneous solution of the electromagnetic and hydrodynamics equations. The final objective is to build

a complete and realistic model of the plasma spray process using as sole input data the spraying parameters fixed by the operator.

References

[1] P. Fauchais, A. Vardelle, B. Dussoubs, Quo vadis thermal spraying, J. Thermal Spray Technol. 1 (2001) 44–66.

[2] H. Herman, S. Sampath, R. McCune, Thermal spray: Current status and future trends, MRS Bull. 25 (7) (2000) 17–25.

[3] R. Westhoff, G. Trapaga, J. Szekely, Plasma particle interactions in plasma spraying system, Metallurg. Trans. B 23 (1992) 683–693.

[4] Y.P. Chyou, E. Pfender, Modelling of plasma jets with superimposed vortex flow, Plasma Chem. Plasma Proces. 9 (2) (1989) 291–328.

[5] C.H. Chang, J.D. Ramshaw, Modeling of non equilibrium effects in a high-velocity nitrogen–hydrogen plasma jet, Plasma Chem. Plasma Proces. 16 (1 Suppl.) (1996) 5S–17S.

[6] J.M. Bauchire, J.J. Gonzales, A. Gleizes, Modelling of DC plasma torch in laminar and turbulent flow, Plasma Chem. Plasma Proces. 17 (4) (1997) 409–432.

[7] M. Vardelle, A. Vardelle, P. Fauchais, M.I. Boulos, Plasma-particle momentum and heat transfer: modeling and measurements, J. AIChE 29 (2) (1983) 236–243.

[8] M. Vardelle, A. Vardelle, P. Fauchais, Particle dynamics and heat transfer under plasma conditions, M.I. Boulos, J. AIChE 34 (4) (1988) 567–573.

[9] P. Eichert, M. Imbert, C. Coddet, Numerical study of an ArH_2 gas mixture flowing inside and outside a dc plasma torch, J. Thermal Spray 7 (1998) 505–511.

[10] B. Liu, T. Zhang, D.T. Gawne, Computational analysis of the influence of process parameters on the flow field of a plasma jet, J. Surface Coatings Technol. 132 (2000) 202–216.

[11] G. Mariaux, E. Legros, A. Vardelle, Modeling of coating formation and heat flux to substrate by particles and plasma jet in plasma spraying, in: Proceedings of the 10th International Ceramics Congress CIMTEC, vol. 3, 2002, p. 341.

[12] S.A. Wutzke, E. Pfender, E.R.G. Eckert, Study of electric ARC behavior with superimposed flow, AIAA J. 5 (1967) 707–714.

[13] Z. Duan, J. Heberlein, Arc instabilities in a plasma spray torch, J. Thermal Spray Technol. 11 (1) (2002) 44–57.

[14] S. Janisson, A. Vardelle, J.F. Coudert, P. Fauchais, E. Meillot, Analysis of the stability of DC plasma gun operating with Ar–He–H_2 gas mixtures, in: Annals of the New York Academy of Sciences, vol. 891, 1999, pp. 407–416.

[15] J.F. Coudert, P. Fauchais, Transient phenomena in d.c. plasma-spray torches, in: Annals of the New York Academy of Sciences, vol. 891, 1991, pp. 382–390.

[16] M.P. Planche, Experimental study of fluctuating plasma jets, Ph.D. Thesis University of Limoges, France, 1995.

[17] O. Betoule, Relationships between the distributions of particle velocity and temperature and coating properties, Ph.D. Thesis, University of Limoges, France, 1994.

[18] O. Lagnoux, Study of particle oxidation under plasma spraying conditions, Ph.D. Thesis, University of Limoges, France, 1999.

[19] J.F. Bisson, B. Gauthier, C. Moreau, Effect of plasma fluctuations on in-flight particle parameters in thermal spray: New Surfaces for a new millennium, in: ASM Int. Materials Park, Berndt, USA, 2001, pp. 715–721.

[20] J.R. Williamson, J.R. Fincke, C.H. Chang, A computational examination of the sources of statistical variances in particle parameters during thermal plasma spraying, Plasma Chem. Plasma Proces. 20 (3) (2000) 115–124.

[21] C. Baudry, A. Vardelle, G. Mariaux, C. Delalondre, E. Meillot, 3-D Modeling of gas flow and particle spray jet in plasma spraying, in: Proceedings of the International Thermal Spray Conference ITSC 2004, Berndt, 2004.

[22] C. Baudry, G. Mariaux, A. Vardelle, C. Delalondre, E. Meillot, Modeling of arc formation in a dc plasma spray torch, in: Proceedings of the 16th International Symposium on Plasma Chemistry ISPC, 2003, CD ROM.

[23] G. Mariaux, E. Legros, A. Vardelle, Modeling of coating formation and heat flux to substrate by particles and plasma jet in plasma spraying, in: Proceedings of the International Thermal Spray Conference ITSC, ASM International, 2003, pp. 895–903.

[24] M. Boulos, P. Fauchais, E. Pfender, Thermal Plasmas: Fundamental and Applications, Plenum Press, New York, 1995.

[25] B. Dussoubs, 3D modeling of the plasma spray process: Influence of the injection conditions of the powder and spraying parameters on the particle treatment and repartition in the flow, Ph.D. Thesis, University of Limoges, France, 1998.

[26] A. Vardelle, H. Zhang, N.J. Themelis, Modeling of in-flight oxidation and evaporation of plasma-sprayed iron particles, in: Proceedings of the 15th International Symposium on Plasma Chemistry ISPC, 2001, pp. 311–318.

[27] Theoretical manual, ESTET v3.1, EDF-Simulog.

[28] J.P. Van Doormal, G.D. Raithby, Enhancement of the simple method for predicting incompressible fluid flows, Numer. Heat Transfer 7 (1984) 147–163.

[29] C.R. Wilke, A viscosity Equation for gas mixtures, J. Chem. Phys. 18 (1950) 517–519.

[30] E.A. Mason, S.C. Saxena, Approximate formula for the thermal conductivity of gas mixture, J. Phys. Fluid (1958) 361–369.

[31] B.E. Launder, B.I. Sharma, Application of the energy dissipation model of turbulence to the calculation of flow near a spinning disc, Lett. Heat Mass Transfer 1 (1974) 131–138.

[32] Y. Zhou, W. David Mc Comb, G. Vahala, Renormalization Group (RG) in turbulence, historical and comparative perspective, ICASE Report n°97-36, 1997, NASA, CR-201718 1-60.

[33] G. Mariaux, P. Fauchais, A. Vardelle, B. Pateyron, Modeling of the plasma pray process: from powder injection to coating formation, J. High Temperature Material Processes 5 (2001) 61–85.

[34] G. Mariaux, C. Baudry, A. Vardelle, 3-D modeling of gas flow and particle spray jet in plasma spraying, in: Proceedings of the International Thermal Spray Conference ITSC, Berndt, 2001, pp. 933–942.

[35] B. Dussoubs, A. Vardelle, G. Mariaux, N.J. Themelis, P. Fauchais, Modeling of plasma spraying of two powders, J. Thermal Spray 10 (1) (2001) 105–110.

[36] H. Schlichting, Boundary Layer Theory, McGraw-Hill, New York, 1968.

[37] J.L. Dorier, M. Gindrat, C. Hollenstein, A. Salito, M. Loch, G. Barbezat, Time-resolved imaging of anodic arc root behaviour during fluctuations of a DC plasma spraying torch, IEEE Trans. Plasma Sci. 29 (3) (2001) 494–501.

[38] P. Eichert, Study of the gas flow inside and outside a plasma spray torch with the PHOENIX^{TM} CFD code, Ph.D. Thesis, University of Besançon, France, 1996.

[39] K. Remesh, H.W. Ng, S.C.M. Yu, Y.C. Lam, Effects of carrier gas flow on particle in-flight characteristics during the plasma spray process with internal injection, in: Proceedings of the 35th National Heat Transfer Conference, Berndt, Anaheim, USA, 2001, pp. 384–484.

[40] V. Arpaci, P. Larsen, Convection Heat Transfer, Prentice-Hall, Englewood Cliffs, NJ, 1984.

[41] H.A. Stine, V.R. Watson, The theoretical enthalpy distribution of air in steady flow along the axis of a direct-current electric arc, NASA T.N.D. 1331 (1962) 1–35.